Proceedings World Geothermal Congress 2023
Beijing, China, April 17 – 21, 2023

# Numerical Investigation of the Effects of Caprock on Subsurface Temperature and Heat Flow Distributions

Hui Wu, Weiwei Ma, Bo Zhang, Jinjiang Zhang

School of Earth and Space Sciences, Peking University, Beijing, China

hui.wu@pku.edu.cn

**Keywords:** Geothermal reservoir, caprock, heat flow, temperature distribution, thermal conductivity.

## ABSTRACT

The efficient exploitation of geothermal reservoirs relies on the understanding of subsurface temperature distribution, which highly depends on the geological conditions of the crust in which the reservoirs reside. A caprock with a relatively low thermal conductivity is essential to the formation of high-temperature geothermal reservoirs. To understand the effects of caprock on subsurface temperature distribution and heat flow profile, we developed a 2D model to simulate the evolution of temperature distribution under continuous heat input from the model bottom. The model involves a sediment layer with a relatively low thermal conductivity on top of a thick granite layer. Radiogenic heat generation is also considered in the granite layer. Both temperature and vertical heat flow are significantly altered by the caprock. The presence of the caprock leads to the increase of the underlying rock temperature and meanwhile the decrease of surface heat flow. Compared with locations without a caprock, a location covered by a caprock exhibits smaller surface heat flow but higher underlying rock temperature. The thicker the caprock layer and the lower the caprock thermal conductivity, the more significant the impacts that the caprock exerts on the temperature and heat flow distributions. Radiogenic heat generation increases both rock temperature and vertical heat flow. The combination of caprock and radiogenic heat generation together leads to a first increasing and then decreasing pattern in the profile of vertical heat flow from the bottom of the radiogenic heat generation domain to the model surface. Results from the current study indicate that the interpretation of field heat flow/temperature measurements and the identification of high temperature geothermal reservoirs should consider realistic geological conditions, especially the existence of caprock layers and the corresponding thermal properties of the caprocks.

## 1. INTRODUCTION

Geothermal reservoirs have been widely exploited around the world to reduce $CO_2$ emissions and mitigate global warming. As a renewable energy, geothermal energy is characterized as an essential alternative to fossil fuels. Geothermal energy can be utilized in different ways depending on reservoir geological conditions. For geothermal reservoirs with relatively low temperatures, the extracted geothermal energy is generally used to heat and cool buildings, while for reservoirs with relatively high temperatures, geothermal energy can be used to generate electricity through geothermal power plants.

A comprehensive understanding of subsurface temperature distribution is important for the identification of exploitable geothermal reservoirs as well as the determination of appropriate technologies to extract geothermal energy from the reservoirs. However, due to the high cost and technical difficulties in directly measuring temperature distribution in deep reservoirs, available field measurements are generally spatially sparse and limited to shallow depths. The evaluation of geothermal resources is normally performed based on simulated temperature results from relatively simple thermal models and measurable surface expressions such as heat flow (Tester et al., 2006; Wang et al., 2012). Currently, surface heat flow data are available in most continental areas and have been used as a key indicator to guide geothermal resource exploration (Davies and Davies, 2010; Jiang et al., 2019; Jolie et al., 2021). According to Pang et al. (2020), areas with surface heat flow larger than 90 $mW/m^2$ have a great potential for geothermal development, while areas with surface heat flow smaller than 50 $mW/m^2$ may not be suitable for geothermal exploitation.

Both surface heat flow and subsurface temperature distribution depend on geological conditions such as crustal structure, strata lithology, thermal properties, radiation intensity, etc. (Ranalli and Rybach, 2005; Yang et al., 2020). Previous studies investigated the effects of various factors on surface heat flow and temperature distribution, such as basement uplift (Wang et al., 1985; Wang et al., 2020), caprock thickness (Lachenbruch and Marshall, 1966; Guo et al., 2019), thermal conductivity (Xiong and Zhang, 1984; Wang et al., 2020), groundwater activity (Andrews-Speed et al., 1984; Rakotoarimanga et al., 1987; Guo et al., 2019), and so on. Among these factors, caprock is considered an indispensable component for the preservation of heat energy and the formation of high-temperature geothermal reservoirs (Zhang et al., 2017; Feng et al., 2018; Guo et al., 2019). Although important insights have been gained regarding the effect of caprock, there still remain some problems that need further investigation. For example, while some 1D models indicated an increasing vertical heat flow from model bottom to top (ground surface) due to radiogenic heat generation (Lin et al., 2022), many field measurements revealed a first increasing and then decreasing pattern from well bottom to head in the profile of vertical heat flow (Kukkonen and Clauser, 1994). Such a heat flow pattern might be attributed to heat refraction due to thermal conductivity contrast between caprock and basement (Kukkonen and Clauser, 1994). Further analysis is required to comprehensively understand the role of caprock on both the vertical heat flow and temperature distributions. Another interesting question that desires additional research is the feasibility of using surface heat flow as an indicator for the identification of potential high-temperature geothermal reservoirs.

The present study aims to investigate the effect of caprock on subsurface temperature distribution as well as the corresponding surface expression, i.e., surface heat flow. A 2D model with a sedimentary layer as caprock is developed to simulate thermal conduction processes from crust-mantle boundary to ground surface. Key parameters of the caprock layer, including thickness and thermal conductivity, are varied to further analyze their impacts on the profiles of temperature and vertical heat flow. The effect of radiogenic

heat generation is also analyzed by assuming a radiogenic area in the shallow crust. In what follows, we first introduce the 2D model and simulation setup in Section 2, and then present the modeling results and provide discussions on the effect of caprock in Section 3.

## 2. MODEL AND SIMULATION SETUP

The dimensions of the 2D model are 100 × 75 km$^2$ (Fig. 1). A 10 × 1.5 km$^2$ caprock layer is assumed at the middle top of the model. The bottom of the model is assumed the boundary between crust and mantle with a uniform mantle heat flow ($Q_m$) of 50 mW/m$^2$. A constant temperature of 20 °C is applied at the top of the model, and the lateral boundaries are assumed adiabatic.

We use GEOSX, an open-source multiphysics simulation platform jointly developed by Lawrence Livermore National Laboratory, Stanford University, and Total Energies (Gross and Mazuyer, 2021), to simulate thermal conduction processes in the model. A typical rock thermal conductivity of 3 W/m/K is assumed in the model except for the caprock whose thermal conductivity is smaller (1 W/m/K). Rock density and specific heat capacity are 2500 kg/m$^3$ and 790 J/kg/K respectively.

A relatively small initial temperature gradient of 6.4 °C/km is assumed, and we model the thermal conduction process for 100 Ma to achieve a stable temperature profile. Note that thermal convection process caused by groundwater activity in shallow crust is not considered in the current study.

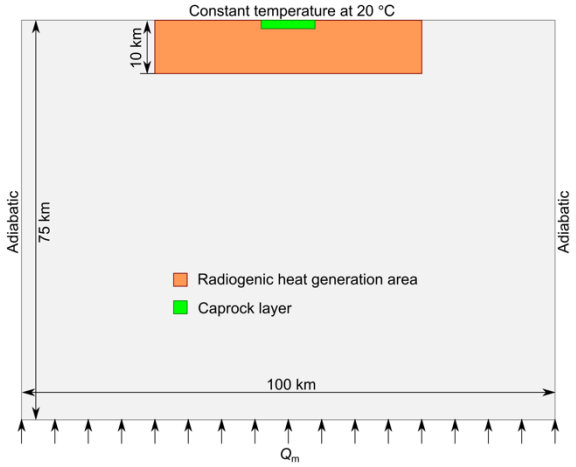


**Figure 1: A 2D thermal model. The radiogenic heat generation domain (orange area) and caprock layer (green area) are annotated. $Q_m$ denotes vertical heat flow from mantle to crust.**

## 3. RESULTS AND DISCUSSION

### 3.1 Temperature and vertical heat flow distributions

The temperature in the model gradually increases due to the heat flux input from the bottom boundary. After 100 Ma, the temperature distribution achieves a stable state as shown in Fig. 2(a). The presence of the caprock layer exhibits considerable impacts on the underlying temperature distribution. At the same depth, rock temperature beneath the caprock (such as the temperature profile at location A in Fig. 2(c)) is higher than that without an overlying caprock (such as the temperature profile at location B in Fig. 2(c)). The temperature gradient is larger within the caprock than that out of the caprock.

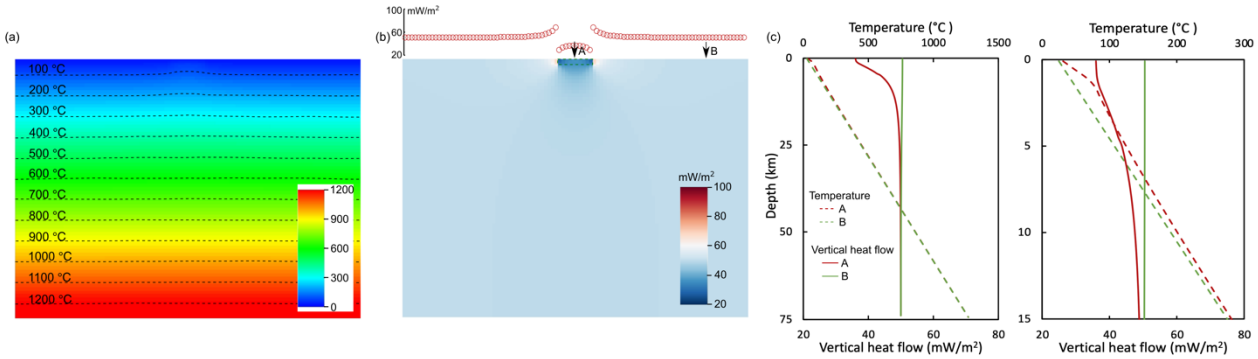


**Figure 2: Simulation results of temperature and vertical heat flow at 100 Ma. (a) Temperature distribution in the model. Isotherms are also annotated. (b) Vertical heat flow in the model. The surface heat flow along the horizontal direction is shown (red circles). (c) Temperature (dashed curves) and vertical heat flow (solid curves) profiles at two locations A and B (annotated in (b)). The right panel further zooms in to show the temperature and vertical heat flow in shallow crust.**

The effect of the caprock on vertical heat flow is more significant than that on temperature (Fig. 2(b)). At the lateral boundary of the model (away from the caprock), the surface heat flow approximately equals the input heat flow from model bottom (50 mW/m$^2$), and

then gradually increases from the lateral boundary towards the caprock. At the boundary of the caprock, the surface heat flow reaches a maximum value of 68.2 mW/m$^2$, and suddenly decreases to a minimum value of 28.3 mW/m$^2$ in the caprock (Fig. 2(b)). The profile of vertical heat flow is also significantly manipulated by the caprock. At location B that is away from the caprock, the vertical heat flow slightly increases from 50 mW/m$^2$ at model bottom to 50.4 mW/m$^2$ at model top. At location A which crosses the caprock, the vertical heat flow gradually decreases from 50 mW/m$^2$ at model bottom to 36 mW/m$^2$ at model top. Note that the vertical heat flow almost remains constant within the caprock.

An interesting observation is that the impact of caprock on vertical heat flow is not limited to the vicinity of the caprock but extends to a rather large depth. As shown in Fig. 2(c), due to the presence of the caprock, the vertical heat flow at location A starts to decrease at a depth of approximately 30 km, which is much larger than the thickness of the caprock layer.

Another important result is that a high surface heat flow does not always indicate a high subsurface temperature. As shown in Fig. 2, the surface heat flow at location A is smaller than that at location B, but the underlying temperature at location A is larger than that at location B. Such a reversed relationship is mainly caused by the caprock which on one hand reduces vertical heat flow, and on the other hand, preserves thermal energy and leads to high rock temperature.

### 3.2 Effect of caprock depth and thermal conductivity

We then vary the thickness of the caprock layer to investigate its effect on subsurface temperature and vertical heat flow distributions (Fig. 3). At location A, with the increase of caprock thickness, the underlying rock temperature increases while the surface heat flow decreases. The surface heat flow for a caprock thickness ($H_c$) of 2.5 km (31.6 mW/m$^2$) is approximately 73% of that for $H_c$ = 0.5 km (43.5 mW/m$^2$), while the temperature at 5 km depth for $H_c$ = 2.5 km (136.2 °C) is 121% of that for $H_c$ = 0.5 km (112.1 °C). At location B that is away from the caprock, the underlying temperature distribution and vertical heat flow are almost identical for the three caprock thicknesses.

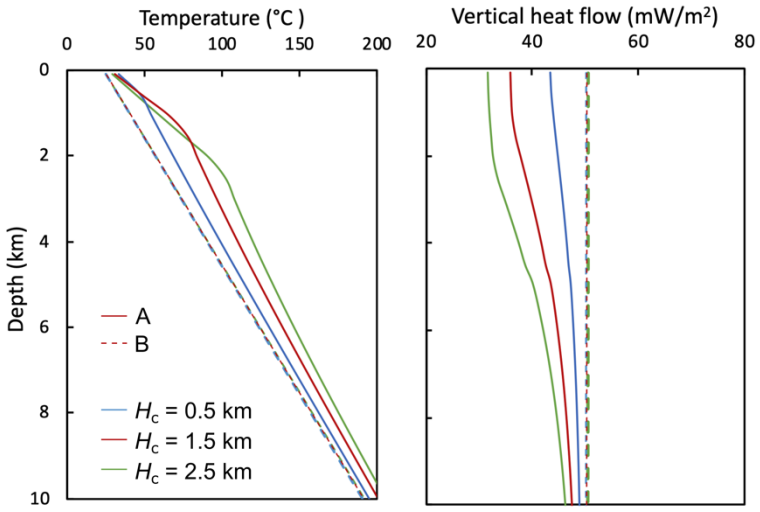


**Figure 3: Comparison of temperature and vertical heat flow with different caprock thickness ($H_c$). We only show the distributions within 10 km depth for clarity.**

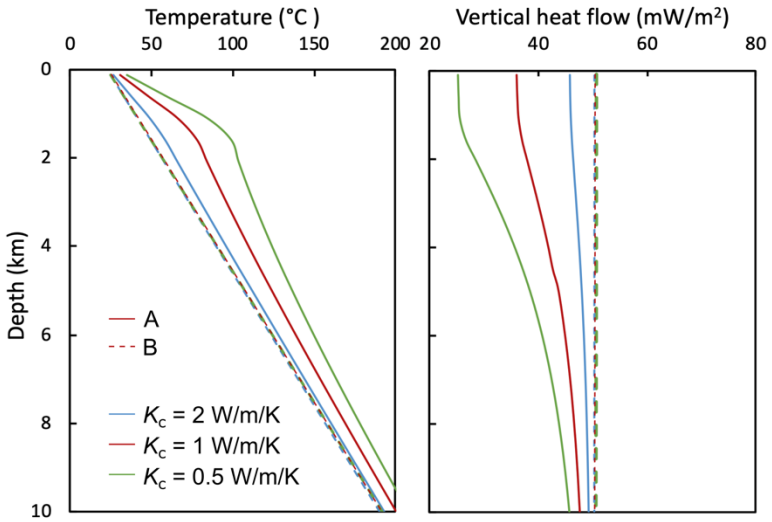


**Figure 4: Comparison of temperature and vertical heat flow with different caprock thermal conductivity ($K_c$).**

The impact of caprock thermal conductivity on temperature and vertical heat flow is similar to that of caprock thickness. With the decrease of caprock thermal conductivity, the contrast in thermal conductivity between the caprock and the underlying rock formation increases, and rock temperature increases while vertical heat flow decreases (Fig. 4). For $K_c$ = 0.5 W/m/K, the surface heat flow at location A (25.1 mW/m$^2$) is only half of that at location B (50.7 mW/m$^2$), but the temperature at 5 km depth at location A (136.7 °C) is 1.27 times of that at location B (107.8 °C).

### 3.3 Combined effect of caprock and radiogenic heat generation

Many field measurements indicated radiogenic heat generation in crust, which may exert a significant impact on both temperature and vertical heat flow. In this section, we consider a radiogenic heat generation area (50 × 10 km$^2$) in the model (annotated by the red dashed square in Fig. 5(b)) with a typical volumetric radiogenic heat generation rate of 2 μW/m$^3$.

The presence of the radiogenic heat generation area leads to larger temperature and vertical heat flow compared with the results in Fig. 2 (Fig. 5). The maximum and minimum surface heat flow still occur at the boundary of the caprock, and the values are 90.4 and 37.1 mW/m$^2$ respectively (Fig. 5(b)). Temperature and vertical heat flow at another location (C) that crosses the radiogenic heat generation area but not the caprock are plotted in Fig. 5(c) for comparison. At location C, the vertical heat flow remains at 50 mW/m$^2$ from model bottom to the bottom of the radiogenic heat generation area, and then increases rapidly to 68.7 mW/m$^2$ at model top. At location A, the vertical heat flow first decreases from 50 mW/m$^2$ at model bottom to 45.2 mW/m$^2$ at the bottom of the radiogenic heat generation area, then increases to 49.1 mW/m$^2$ at approximately 4.5 km depth, and then decreases to 46.9 mW/m$^2$ at model top. Such a complex profile is the result of the combined effects of radiogenic heat generation which increases vertical heat flow and caprock which tends to reduce the underlying vertical heat flow. Field measurements at the Kola deep hole showed similar variation that the vertical heat flow first increased from 45.6 mW/m$^2$ at 7200-9456 m depth to 67.5 mW/m$^2$ at 4500-4900 m depth, and then decreased to 29.7 mW/m$^2$ at 0-1200 m depth (Kukkonen and Clauser, 1994).

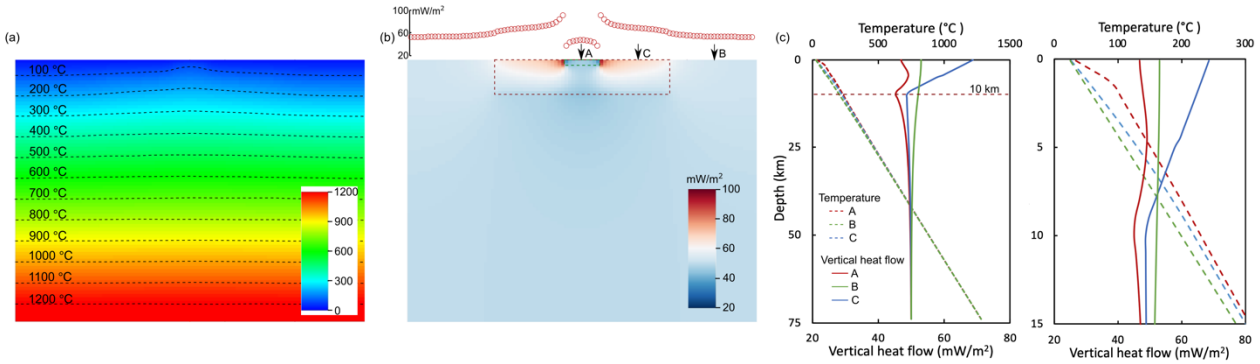


**Figure 5: Simulation results of temperature and vertical heat flow at 100 Ma with radiogenic heat generation.**

We then vary the radiogenic heat generation rate to further understand the combined effect of caprock and radiogenic heat generation (Fig. 6). With the increase of radiogenic heat generation rate *a*, both the temperature and vertical heat flow increase. At location A, the vertical heat flow profile shows the same pattern for all the three radiogenic heat generation rates, i.e., first decreases from model bottom to the bottom of the radiogenic heat generation area, then increases until reaching a turning point (annotated in Fig. 6), and finally decreases from the turning point towards model top. With the increase of *a*, the depth of the turning point decreases. For *a* = 1 μW/m$^3$, the effect of caprock is more significant than that of radiogenic heat generation, while for *a* = 3 μW/m$^3$, the effect of radiogenic heat generation becomes dominant and the turning point moves inside the caprock layer.

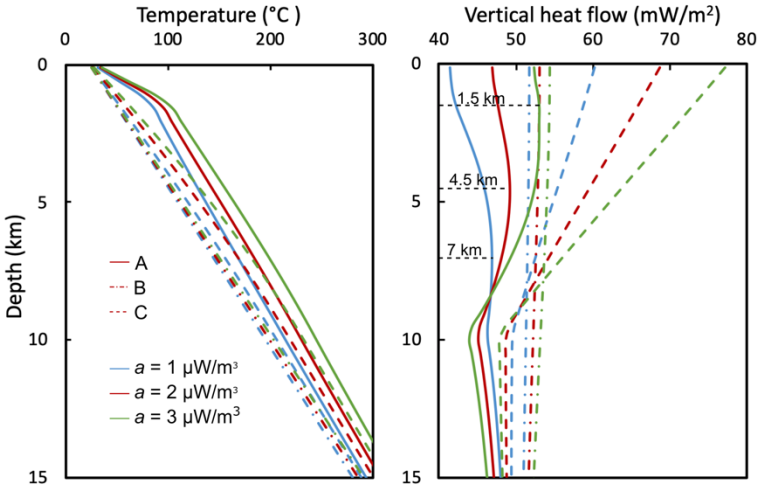


**Figure 6: Comparison of temperature and vertical heat flow with different radiogenic heat generation rate (*a*). The depth of the turning point within the radiogenic heat generation area is annotated.**

## 4. CONCLUSIONS

We investigated the effect of caprock on subsurface temperature and vertical heat flow distributions through a 2D thermal conduction model. Due to the relatively low thermal conductivity of the caprock, vertical heat flow in the caprock is inhibited, leading to a relatively small surface heat flow and a large temperature gradient in the caprock. While the effect of the caprock on temperature distribution is limited within the caprock, its effect on vertical heat flow may extend to areas much deeper than the caprock.

A higher surface heat flow does not always indicate a higher subsurface rock temperature. Compared with locations without a caprock, locations covered by a caprock shows smaller surface heat flow but higher temperature in the underlying rock formations. Therefore, the identification of high temperature geothermal reservoirs should consider both heat flow/temperature measurements and realistic geological conditions. The presence of a caprock layer might be an important indicator of promising geothermal resources.

Different from the effect of caprock, the presence of radiogenic heat generation induces the increase of both temperature and vertical heat flow. The combination of caprock and radiogenic heat generation leads to a complex vertical heat flow profile in the underlying rock formations. The interpretation of field heat flow measurements needs to consider the effect of caprock as well as radiogenic heat generation.

## ACKNOWLEDGEMENT

The authors would like to greatly acknowledge the National Key Research and Development Program of China (No. 2021YFA0716000) and the China National Petroleum Corporation-Peking University Strategic Cooperation Project of Fundamental Research.

## REFERENCES

Andrews-Speed, C.P., Oxburgh, E.R., Cooper, B.A.: Temperatures and depth-dependent heat flow in Western North Sea, American Association of Petroleum Geologists Bulletin, **68**(**11**), (1984), 1764-1781.

Davies, J.H., Davies, D.R.: Earth's surface heat flux, Solid Earth, **1**(**1**), (2010), 5-24.

Feng, Y., Zhang, X., Zhang, B., Liu, J., Wang, Y., Jia, D., et al.: The geothermal formation mechanism in the Gonghe Basin: Discussion and analysis from the geological background, China Geology, **1**(**3**), (2018), 331-345.

Gross, H., Mazuyer, A.: GEOSX: A Multiphysics, Multilevel Simulator Designed for Exascale Computing, SPE Reservoir Simulation Conference, SPE, On-Demand, SPE-203932-MS (2021).

Guo, S., Zhu, C., Qiu, N., Tang, B., Cui, Y., Zhang, J., and Zhao, Y.: Present geothermal characteristics and influencing factors in the Xiong'an new area, North China, Energies, **12**(**20**), (2019), 3884.

Jiang, G., Hu, S., Shi, Y., Zhang, C., Wang, Z., Hu, D.: Terrestrial heat flow of continental China: Updated dataset and tectonic implications, Tectonophysics, **753**, (2019), 36-48.

Jolie, E., Scott, S., Faulds, J., Chambefort, I., Axelsson, G., Gutiérrez-Negrín, L.C., et al.: Geological controls on geothermal resources for power generation, Nature Reviews Earth and Environment, **2**(**5**), (2021), 324-339.

Kukkonen, I.T., Clauser, C.: Simulation of heat transfer at the Kola deep-hole site: implications for advection, heat refraction and palaeoclimatic effects, Geophysical Journal International, **116**(**2**), (1994), 409-420.

Lachenbruch, A.H., Marshall, B.V.: Heat flow through the Arctic Ocean floor: The Canada Basin-Alpha Rise Boundary, Journal of Geophysical Research, **71**(**4**), (1966), 1223-1248.

Lin, W., Wang, G., Gan, H., Zhang, S., Zhao, Z., Yue, G., et al.: Heat source model for Enhanced Geothermal Systems ( EGS ) under different geological conditions in China, Gondwana Research, in press (2022).

Pang, Z., Luo, J., Cheng, Y., Duan, Z., Tian, J., Kong, Y., et al.: Evaluation of geological conditions for the development of deep geothermal energy in China, Earth Science Frontiers, **27**(**1**), (2020), 134-151.

Rakotoarimanga, Celati, R., Taffi, L., Squarci, P., and Calore, C.: Surface heat flow and deep temperatures in the Bradano Trough (Southern Italy). Possible effects of groundwater circulation, Geothermics, **16**, (1987), 473-485.

Ranalli, G., Rybach, L.: Heat flow, heat transfer and lithosphere rheology in geothermal areas: Features and examples, Journal of Volcanology and Geothermal Research, **148**, (2005), 3-19.

Tester, J.W., Anderson, B., Batchelor, A., Blackwell, D., DiPippo, R., Drake, E., et al.: The future of geothermal energy: impact of Enhanced Geothermal Systems (EGS) on the United States in the 21st Century, Final report to the US Department of Energy Geothermal Technologies Program, (2006).

Wang, J., Hu, S., Pang, Z., He, L., Zhao, P., Zhu, C., et al.: Estimate of geothermal resources potential for hot dry rock in the continental area of China, Science and Technology Review, **30**(**32**), (2012), 25-31.

Wang, J., Wang, J., Xiong, L., and Zhang, J.: Analysis of factors affecting heat flow density determination in the Liaohe Basin, North China, Tectonophysics, **121**, (1985), 63-78.

Wang, X., Mao, X., Mao, X., Li, K.: Characteristics and Classification of the Geothermal Gradient in the Beijing–Tianjin–Hebei Plain, China, Mathematical Geosciences, **52**(**6**), (2020), 783-800.

Xiong, L., and Zhang, J.: Mathematical simulation of refract and redistribution of heat flow, Chinese Journal of Geology, **19**(**4**), (1984), 445-454.

Yang, W., Han, S., and Li, W.: Geological factors controlling deep geothermal anomalies in the Qianjiaying Mine, China, International Journal of Mining Science and Technology, **30**(**6**), (2020), 839-847.

Zhang, Y., Feng, J., He, Z., and Li, P.: Classification of geothermal systems and their formation key factors, Earth Science Frontiers, **24**(**3**), (2017), 190-198.